**Advances in Nano Research**, *Vol. 17, No.4 (2024) 323-334*
https://doi.org/10.12989/anr.2024.17.4.323


# Nonlinear FG-CNT effect on the critical buckling load of nanocomposite beams with different boundary conditions

Youcef Tlidji*[1], Mohamed Zidour[2], Rachid Zerrouki[2], Abdelillah Benahmed[2,3], Boumediene Serbah[4,5], Kada Draiche[5,6] and Khaled Bouakkaz[1]

[1]*Materials and Structures Laboratory, Civil Engineering Department, University of Tiaret, Algeria*
[2]*Laboratory of Geomatics and Sustainable Development, University of Tiaret, Algeria*
[3]*Department of Physique, University of Blida 1,270 BP Route Soumâa -BLIDA-, Algeria*
[4]*Water and Works in Their Environment Laboratory (EOLE), University of Tlemcen, BP 230, 13000, Algeria*
[5]*Civil Engineering Department, University of Tiaret, Algeria*
[6]*Material and Hydrology Laboratory, Civil Engineering Department, Faculty of Technology, University of Sidi Bel Abbes, SidiBel Abbes, Algeria*

(*Received May 10, 2024, Revised September 15, 2024, Accepted September 19, 2024*)

**Abstract.** This paper deals with the effect of non-linear volume fraction distribution of carbon nanotube in the FG-CNTRC beams on the critical buckling via a hyperbolic shear deformation theory. Here, different boundary condition was considered including hinged hinged, clamped clamped and clamped-free. Single-walled carbon nanotubes are aligned and distributed in the polymer matrix in different ways to reinforce it and the material properties of (CNTRC) beams are assumed to vary gradually along the thickness direction, following a new exponential power law distribution of (CNT). The effective material properties of nanocomposite beams are estimated using the rule of mixture. The governing equations of the mathematical models are obtained by applying Hamilton's principle. The results provided of mathematical models in this work are compared and validated with similar ones in the literature. The critical buckling loads of nanocomposite beams with different boundary conditions of linear and non-linear distribution of CNT volume fraction were obtained. The effects of several parameters, including the type of beam, the volume fraction of carbon nanotubes (CNTs), the exponent degree (n), and the aspect ratio, were investigated. The distribution non-linearity of CNT volume fraction in the beam has a significant impact on the mechanical properties, particularly in buckling behavior with different boundary conditions.

**Keywords:** boundary conditions; critical buckling; FG-CNT; nanotube; non-linear; volume fraction

## 1. Introduction

Since their discovery by Iijima in 1991 (Iijima 1991), carbon nanotubes have been increasingly used due to their excellent electronic, thermal, and mechanical properties. (Dresselhaus 2001). Other studies have shown that they can be used for nano-electronics, nano-tools, and nanocomposite (Zhang *et al*. 2016, Ebrahimi and Habibi 2017). Carbon nanotubes have excellent electronic and mechanical properties, such as their extremely high elastic modulus, tensile strength, aspect ratio, and low density. These properties make them an excellent candidate for the reinforcement of polymer composites.

Due to the challenges faced in experimental methods and MD simulations (Jin and Yuan 2003) for predicting nanostructure responses under different loading conditions. The continuum mechanics methods are commonly used to investigate physical phenomena at the nanoscale. (Ru 2000). Recently, the continuum mechanics approach has been shown to be effective in predicting the responses of nanostructures. Vodenitcharova and Zhang (2006) discovered the bending and buckling of a nanocomposite beam using the continuum mechanics model. Peddieson *et al*. (2003) used the nonlocal continuum models to nanotechnology. The continuum mechanics approach has been used to study a wide range of phenomena in recent research such as statics (Weon 2009, Eltaher *et al*. 2019), the buckling (She *et al*. 2017, Wang *et al*. 2006), free vibration (Alhaifi *et al*. 2023), boundary conditions (Zenkour 2018).

In mathematics modeling, the boundary conditions are constraints that are imposed on the solution of a differential equation at the boundary of the domain over which the equation is defined. Boundary conditions make the solution of the differential equation well-behaved. Yas and Samadi (2012) investigate the natural frequency and critical buckling load of CNTRC beams with or without an elastic foundation for various boundary conditions using the differential quadrature method and Hamilton's principle. Zenkour (2018) discovered a modified couple stress theory for micro-machined beam with various boundary conditions and linearly varying thickness. The influences of volume fraction of CNT and boundary conditions on the buckling of column have been investigated by Arani and Kolahchi (2016).

FGMs, a new class of composite materials with a graded composition, have recently attracted significant attention

*Corresponding author, Ph.D.,
E-mail: youcef.tlidji@univ-tiaret.dz



ISSN: 2287-237X (Print), 2287-2388 (Online)

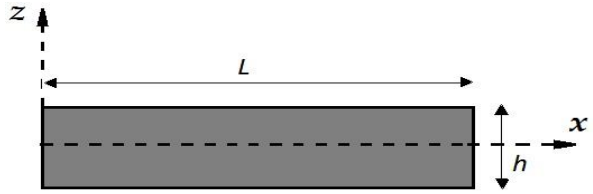


**Fig. 1 Geometry of FG-CNTRC beamt**

from researchers. (Heidari *et al*. 2020, Jamali *et al*. 2019, Zghal *et al*. 2020, Chang and Li 2024, Chang *et al*. 2024). The functionally graded concept was first used in 2009 to study the mechanical static behavior of the graded carbon nanotube reinforced composite (CNTRC) (Shen 2009). A systematic model for the mechanical behavior of thin-walled composite FGM pipelines has been studied by Zhang *et al*. (2024). Li *et al*. (2023) investigate the buckling of the encased functionally graded porous composite liner with polyhedral shapes reinforced by graphene platelets under external pressure.

Mohammadimehr *et al*. (2017) investigated the nonlinear vibration of a functionally graded (FG) carbon nanotube reinforced composite (CNTRC) sandwich Timoshenko beam subjected to a longitudinal magnetic field using the modified couple stress theory and the generalized differential quadrature method. The bending, buckling, and vibration behavior of the graded CNT reinforced beam were further estimated under a non-uniform temperature load. (Mayandi and Jeyaraj 2015). Mellouli *et al*. (2020) investigated the free vibration of functionally graded carbon nanotubes-reinforced beams using the modified first-order shear deformation theory and the mesh free radial point interpolation method.

Yang *et al*. (2015) investigated the dynamic buckling of functionally graded nanocomposite beams (FG-CNTR) reinforced by carbon nanotubes (CNT) as a core and incorporeal with two surface bonded piezoelectric layers. Wu *et al*. (2015) studied the free vibration and buckling behavior of sandwich beams reinforced with functionally graded carbon nanotube-reinforced composite (FG-CNTRC) face sheets using Timoshenko beam theory.

Many studies exist in the literature, in terms of composite materials (Phung-Van *et al*. 2018, Xiao *et al*. 2023, Zhang *et al*. 2015). Xiao *et al*. (2024) studied a structural optimization model of confined polyhedral composite subsea pipelines under pressure and thermal fields. The nanocomposites have been increasingly analyzed (Kiani 2017, Kolahchi *et al*. 2020, Mehar and Panda 2018, Mirzaei and Kiani 2016, Mallek *et al*. 2020, Xiao *et al*. (2022) investigated the nonlinear in-plane instability of the confined FGP arches with nanocomposites reinforcement.

The volume fraction of CNTs in a composite material is the proportion of the volume occupied by the CNTs to the total volume of the material. The CNT volume fraction is a key factor that influences the properties of the composite material, such as its strength, stiffness, and thermal conductivity. The maximum CNT volume fraction can be added to a composite material depends on a number of factors, including the type of CNTs, the type of matrix, and the manufacturing process. In general, the maximum CNT volume fraction is limited by the ability of the CNTs to disperse evenly in the matrix and the CNTs to bond to the matrix. Jiang *et al*. (2009) investigated the Maximum nanotube volume fraction and its effect on overall elastic properties of nanotube-reinforced composites. He concluded that the maximum CNT volume fraction is determined by the CNT geometry, the surface-to-surface distance between adjacent CNTs, and the CNT packing pattern. Since the diameter of CNTs is comparable to the equilibrium van der Waals distance, increasing the surface-to-surface distance and/or decreasing the CNT diameter will significantly reduce the maximum CNT volume fraction.

In this paper, we focus on the nonlinear distribution of CNTs in FG-CNTRC beams with different boundary conditions. the higher-order shear deformation theories are used to accurately formulate the influences of the transverse shear stress distribution along the beam thickness. The linear distribution of CNT used in the previous studies has been replaced by nonlinear distribution to analyze the critical buckling load. In this regard, the CNT volume fraction distribution law is considered exponential. This equation captures the impact of nonlinear distribution on both mechanical and economic aspects. On the mechanical side, the nonlinear distribution of CNTs has demonstrated a notable increase in the beam's rigidity compared to the linear distribution. It is crucial to note that this enhancement in rigidity is achieved with the same quantity of CNTs used in both linear and nonlinear distributions. This underscores the significance of nonlinear distribution from an economic standpoint. Additionally, economic benefits can be realized, for instance by improving the mechanical properties of the beam by increasing the exponent (n) rather than raising the volume fraction of CNTs. The effect of different parameters on the buckling analysis such as aspect ratios, volume fraction, and order of the exponent of volume fraction law distribution are studied and discussed.

## 2. Configuration of FG-CNTRC beams and volume fraction CNT distribution

Let us consider a FG-CNTRC rectangular beam with different boundary conditions. The respective length and thickness of FGM beam are represented by L and h with the coordinate system (x, z) shown in Fig. 1. The CNTRC are made of SWCNTs embedded in the isotropic matrix with linear (n=1) and non-linear (n>1) volume fraction distribution shown in Figs. 2 and 3 respectively.

The mathematical form of the relationship between the CNT volume fraction and distribution configuration is presented in Table 1. Where (n) the exponent degree of Carbone nanotube volume fraction equation and $V_{cnt}^{*}$ is the volume fraction of Carbone nanotube, which can be calculated from the equation.

$$V_{cnt}^{*} = \frac{W_{cnt}}{W_{cnt} + (\rho^{cnt}/\rho^{p})(1 - W_{cnt})} \tag{1}$$

In which $W_{cnt}$ is the CNT mass fraction, $\rho^{cnt}$ is the CNT density, and $\rho^{P}$ is the polymer density in CNTRC

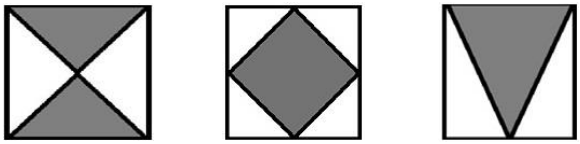

**X-beam** O-beam V-beam

**Fig. 2 Cross sections of different types of FG-CNTRC with linear distribution (n=1)**

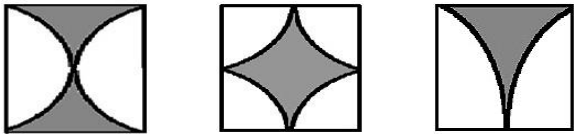

**X-beam** O-beam V-beam

**Fig. 3 Cross sections of different types of FG-CNTRC with non-linear distribution (n<1)**

beams. When the exponent degree n=0, the carbon nanotubes (CNTs) are distributed uniformly in the matrix (UD-CNTs) and when the exponent degree n=1, the CNTs are distributed linearly. The distribution of CNTs is non-linear for all values of n greater than 1.

The rule of mixture model is used to calculate the Young's modulus and shear modulus of FG-CNTRC materials. (Shen 2009)

$$E_{11} = \eta_1 V_{cnt} E_{11}^{cnt} + V_p E^p \tag{2a}$$

$$\frac{\eta_2}{E_{22}} = \frac{V_{cnt}}{E_{22}^{cnt}} + \frac{V_p}{E^p} \tag{2b}$$

$$G_{12}\frac{\eta_3}{G_{12}} = \frac{V_{cnt}}{G_{12}^{cnt}} + \frac{V_p}{G^p} \tag{2c}$$

where $V_{cnt}$ and $V_p$ are the CNT and polymer volume fractions respectively. Furthermore, $E_{11}^{cnt}$, $E_{22}^{cnt}$ and $G_{12}^{cnt}$ are the Young modulus and shear modulus of SWCNTs, respectively. $E^p$ and $G^p$ Specify the material properties of the isotropic matrix. Based on the rule of mixture and MD simulations given by Han and Elliott (2007), Yas and Samadi (2012) Proposed three efficiency parameters that can be used to model the size-dependent properties of CNTRC beams. Table 2 shows the efficiency parameters related to the volume fraction $(V_{cnt}^*)$.

The rule of mixture is used to calculate the mass density and Poisson's ratio of the FG-CNTRC beams, with the following results:

$$\rho = V_{cnt}\rho^{cnt} + V_p\rho^p \tag{3}$$

$$\nu_{12} = V_{cnt}\nu_{12}^{cnt} + V_p\nu^p \tag{4}$$

## 3. Equations of motion

Assuming that the FG beam deform in two dimensions plane only$(x, z)$, we can define $u(x, z)$ and $w(x, z)$ as the displacements field of this theory of any point in the beam along the *x* and *z* axes Simsek (2010). These components can be expressed using Eq. (5) as follows:

Table 1 The mathematical form of the CNT volume fraction distribution configuration

| | $V_{cnt}$ |
|---|---|
| X-beam | $(n+1)(2\frac{\lvert z\rvert}{h})^n V_{cnt}^*$ |
| O-beam | $(n+1)(1-2\frac{\lvert z\rvert}{h})^n V_{cnt}^*$ |
| V-beam | $(n+1)(\frac{1}{2}+\frac{z}{h})^n V_{cnt}^*$ |

Table 2 The CNT efficiency parameters ($\eta$)

| case | $\eta_1$ | $\eta_2 = \eta_3$ |
|---|---|---|
| $V_{cnt}^*$=0.12 | 1.2833 | 1.0566 |
| $V_{cnt}^*$=0.17 | 1.3414 | 1.7101 |
| $V_{cnt}^*$=0.28 | 1.3238 | 1.7380 |

$$\begin{aligned} u(x,z,t) &= U - zw' + f(z)\phi \\ w(x,z,t) &= W \end{aligned} \tag{5}$$

where $f(z) = \frac{2z(tansh(1)^2-1)+h\,tanh(2z/h)}{2\,tanh(1)^2}$

The shape function considered in this paper as proposed by Belarbi *et al.* (2023). The displacement components of a point on the neutral axis of the beam along the x and z directions are represented by $U = U(x,t)$ and $W = W(x,t)$, respectively, while $\phi = \phi(x,t)$ denote the rotational angle of the cross-section about the y-axis compared to its undeformed position. For conciseness, the prime symbol (') indicates the partial differentiation of the quantities with respect to x.

The strains associated with the displacement field in Eq. (5) are as follows:

$$\varepsilon_x = \frac{\partial u}{\partial x} = U' - zW'' + f(z)\phi' \tag{6a}$$

$$\gamma_{xz} = \frac{\partial u}{\partial z} + \frac{\partial w}{\partial x} = \frac{df(z)}{dz}\phi \tag{6b}$$

The virtual work principle is utilized to derive the governing equations of buckling loads and boundary conditions. (Kiani *et al*. 2011):

$$\delta U + \delta V = 0 \tag{7}$$

In which δU is the virtual variation strain energy of the beam which calculated by:

$$\begin{aligned} \delta U &= \int_0^L \int_0^b \left[\int_{h_{n1}}^{h_n} (\sigma_x \delta\varepsilon_x + \sigma_{xz}\delta\gamma_{xz})dzdydx\right] \\ &= \int_0^L \left\{N_x\delta U' - M_x\delta W'' + P_x\delta\phi' + Q_{xz}\frac{df(z)}{dz}\delta\phi\right\}dx \end{aligned} \tag{8}$$

where $N_x$, $M_x$, $P_x$, and $Q_{xz}$ denote the stress resultants defined and they are defined by:

$$\begin{aligned} (N_x, M_x, P_x) &= \textstyle\int_{-h/2}^{h/2}(b, zb, fb)\sigma_x dz, \\ Q_{xz} &= \int_{-h/2}^{h/2}\sigma_{xz}\frac{df(z)}{dz}bdz \end{aligned} \tag{9}$$

The variation of potential energy $\delta V$ of the axial compressive loads which induce the geometrical instability

state of the beam can be expressed:

$$\delta V = -\int_{-\frac{L}{2}}^{\frac{L}{2}} P_0 w' \delta w' \tag{10}$$

## 4. Linear constitutive relations

The linear constitutive relationship between stress and strain for elastic functionally graded (FG) beams can be expressed in the following manner:

$$\begin{aligned} \sigma_x &= E\varepsilon_x \\ \sigma_{xz} &= \frac{E}{2[1+\nu]}\gamma_{xz} \end{aligned} \tag{11}$$

By incorporating Eq. (6) into Eq. (11), the stress resultants can be expressed as follows:

$$\begin{Bmatrix} N_x \\ M_x \\ P_x \\ Q_{xz} \end{Bmatrix} = \begin{bmatrix} A & B & C & 0 \\ B & D & F & 0 \\ C & F & H & 0 \\ 0 & 0 & 0 & A_s \end{bmatrix} \begin{Bmatrix} U' \\ -W'' \\ \phi' \\ \phi \end{Bmatrix} \tag{12}$$

where stiffness components are given as:

$$(A, B, D, C, F, H) = \int_A E(1, z, z^2, f, zf, f^2) dA \tag{13}$$

$$A_s = \int_A \frac{E}{2(1+\upsilon)} \left(\frac{df}{dz}\right)^2 dA \tag{14}$$

Upon substitution the expressions of Eqs. (8) and (10) into Eq. (7) and integrating the equation by parts, and gathering the coefficients associated with $\delta U$, $\delta\phi$ and $\delta W$, the overall equations of motion of the CNTRC beam can be written:

$$N_x' = 0 \tag{15q}$$

$$M_x'' - P_0 W'' = 0 \tag{15b}$$

$$P_x' - Q_{xz} = 0 \tag{15c}$$

The displacement components can be expressed using the state space approach Tlidji *et al*. (2022).

$$\begin{Bmatrix} U(x,t) \\ \phi(x,t) \\ W(x,t) \end{Bmatrix} = \begin{bmatrix} U(x) \\ \phi(x) \\ W(x) \end{bmatrix} \tag{16}$$

where $\omega$ is the eigen-frequency. A system of ordinary differential equations is obtained by substituting Eq. (16) into Eq. (15).

$$\begin{aligned} U'' &= b_1 U + b_2 W'' \\ \phi'' &= b_3 \phi + b_4 W'' \\ W^{iv} &= b_5 \phi' + b_6 W'' \end{aligned} \tag{17}$$

where the $b_n$ are the constants coefficients

$$\begin{aligned} b_1 &= \frac{-CA_s}{AH - C^2}, & b_2 &= \frac{BH - CF}{AH - C^2}, \\ b_3 &= \frac{AA_s}{AH - C^2}, & b_4 &= \frac{AF - BC}{AH - C^2}, \\ b_5 &= \frac{Bb_1 - Fb_3}{Bb_2 - Fb_4 - D}, & b_6 &= \frac{P_0}{Bb_2 - Fb_4 - D} \end{aligned} \tag{18}$$

The systems of Eqs. (17) can be converted into a matrix form as:

$$Z'(x) = TZ(x) \tag{19}$$

where

$Z(x) = \{\phi, \phi', W, W', W''\}$. and matrix T is defined as:

$$T = \begin{bmatrix} 0 & 1 & 0 & 0 & 0 & 0 \\ b_3 & 0 & 0 & 0 & 0 & b_4 \\ 0 & 0 & 0 & 1 & 0 & 0 \\ 0 & 0 & 0 & 0 & 1 & 0 \\ 0 & 0 & 0 & 0 & 0 & 1 \\ 0 & b_5 & 0 & 0 & b_6 & 0 \end{bmatrix} \tag{20}$$

A formal solution of Eq. (20) is given by:

$$Z(x) = e^{Tx} K \tag{21}$$

where $K$ is a constant column vector determined from the boundary conditions at $x = \pm L/2$; and $e^{Tx}$ is the general matrix solution of Eq. (21) which is given as:

$$e^{Tx} = [E] \begin{bmatrix} 1 & x & 0 & 0 & 0 & 0 \\ x & 1 & 0 & 0 & 0 & 0 \\ 0 & 0 & e^{\lambda_3 x} & 0 & 0 & 0 \\ 0 & 0 & 0 & e^{\lambda_4 x} & 0 & 0 \\ 0 & 0 & 0 & 0 & e^{\lambda_5 x} & 0 \\ 0 & 0 & 0 & 0 & 0 & e^{\lambda_6 x} \end{bmatrix} [E]^{-1} \tag{22}$$

where $\lambda_i (i = \overline{1,n} = \overline{1,6})$ and $[E]$ are eigenvalues and corresponding matrix of eigenvectors, respectively, associated with the matrix $T$.

## 5. Analytical solution under various boundary conditions

The exact solution for the FG beam under various boundary conditions can be constructed.

In terms of the unknown function Z(x), the boundary conditions can be expressed as follows:

Clamped (C): $\phi = W = W' = 0$ (23a)

Pinned (S): $\phi = \phi' = W'' = 0$ (23b)

Free (F): $\phi' = W'' = (Bb_2 + Fb_6)\phi - P_0 W' + (Bb_4 + Fb_8 - D)W'''\phi'' = 0$ (23c)

Substituting Eq. (21) into Eqs. (23), a homogeneous system of equations is obtained as:

$$G_{ij} \rightleftarrows K_i = 0, \ (i = 1..6), (j = 1..6) \tag{23d}$$

where

$$[G(x)] = [E] \begin{bmatrix} 1 & x & 0 & 0 & 0 & 0 \\ x & 1 & 0 & 0 & 0 & 0 \\ 0 & 0 & e^{\lambda_3 x} & 0 & 0 & 0 \\ 0 & 0 & 0 & e^{\lambda_4 x} & 0 & 0 \\ 0 & 0 & 0 & 0 & e^{\lambda_5 x} & 0 \\ 0 & 0 & 0 & 0 & 0 & e^{\lambda_6 x} \end{bmatrix} [E]^{-1} \tag{24}$$

The buckling load can be determined by setting the determinant of $G_{ij}$ to zero. It is important to note that a trial and error procedure is required to obtain the buckling

Table 3 Non-dimensional critical buckling load $(\bar{N}_{cr})$ of S-S FG-CNTRC beams with different *L/h* values

| L/h | $V_{cnt}^{*}$ | Reference | Beam | | |
|---|---|---|---|---|---|
| | | | UD | X | O |
| 10 | 0.12 | Present | 0.1655 | 0.2027 | 0.1049 |
| | | Belarbi *et al.* 2023 | 0.1655 | 0.2082 | 0.1049 |
| | 0.17 | Present | 0.2593 | 0.3183 | 0.1620 |
| | | Belarbi *et al.* 2023 | 0.2593 | 0.3260 | 0.1620 |
| | 0.28 | Present | 0.3584 | 0.4125 | 0.2414 |
| | | Belarbi *et al.* 2023 | 0.3584 | 0.4270 | 0.2414 |
| 15 | 0.12 | Present | 0.0988 | 0.1291 | 0.0574 |
| | | Belarbi *et al.* 2023 | 0.0988 | 0.1314 | 0.0574 |
| | | Yas and Samadi 2012 | 0.0986 | 0.1288 | 0.0588 |
| | | Zerrouki *et al.* 2020 | 0.0984 | 0.1289 | 0.0576 |
| | | Tagrara *et al.* 2015 | 0.0985 | 0.1291 | 0.0575 |
| | 0.17 | Present | 0.1507 | 0.1989 | 0.0862 |
| | | Belarbi *et al.* 2023 | 0.1506 | 0.2011 | 0.0862 |
| | | Yas and Samadi 2012 | 0.1505 | 0.1999 | 0.0877 |
| | | Zerrouki *et al.* 2020 | - | 0.1979 | 0.0864 |
| | 0.28 | Present | 0.2206 | 0.2767 | 0.1324 |
| | | Belarbi *et al.* 2023 | 0.2206 | 0.2811 | 0.1324 |
| | | Yas and Samadi 2012 | 0.2209 | 0.2896 | 0.1337 |
| 20 | 0.12 | Present | 0.0633 | 0.0866 | 0.0351 |
| | | Belarbi *et al.* 2023 | 0.0630 | 0.0630 | 0.0351 |
| | 0.17 | Present | 0.0951 | 0.1307 | 0.0521 |
| | | Belarbi *et al.* 2023 | 0.0946 | 0.0946 | 0.0521 |
| | 0.28 | Present | 0.1437 | 0.1903 | 0.0812 |
| | | Belarbi *et al.* 2023 | 0.1430 | 0.1430 | 0.0812 |

load values due to the presence of unknown $P_0$ in matrix $T$.

The following iteration procedure has been used to calculate the buckling load P0:

Step 1: Assign a small initial value of P0.

Step 2: Form matrix T and compute the eigenvalues $\lambda_i$ and eigenvectors [E] of T

Step 3. Form matrix [G] according to appropriate boundary conditions in Eqs. (23a–23c)

Step 4. Check if the determinant of matrix [G] changes sign.

(a) If no, increase the buckling load and go back to Step 2.

(b) If yes, decrease the buckling load by a small amount and go to next step.

Step 5. Check if the relative error between two successive iterations is within a given tolerance, stop the iteration. Otherwise, return to Step 2.

## 6. Buckling behaviors results and discussion

In this research, analyses of critical buckling behavior of FG-CNTRC beams are investigated. Mechanical properties of nanocomposite FG-CNTRC beam made of CNT reinforced Polymetyl- methacrylate, referred as (PMMA) where $\upsilon^{p} = 0.3$, $\rho^{p} = 1190\text{Kg/m}^3$, and $E^{p} = 2.5\text{GPa}$ indicate the corresponding properties for the PMMA matrix. For reinforcement material, the armchair (10,10) SWCNTs is chosen with the following properties according to the study of Zhu *et al.* (2012): $\upsilon^{cnt} = 0.19, \rho^{cnt} = 1400\text{Kg/m}^3$, $E_{11}^{cnt} = 600\text{GPa}$, $E_{22}^{cnt} = 10\text{GPa}$, and $G_{12}^{cnt} = 17.2\text{GPa}$.

Dimensionless parameters for buckling analysis are used:

$$\bar{N}_{cr} = \frac{N_{x0}}{A_{110}} \tag{25}$$

Dimensionless critical buckling load of FG-CNTRC beam has been presented in this study. In this work, the obtained results of the dimensionless critical buckling load with different boundary conditions by the analytical methods based on higher order shear deformation theory (HSDT) are compared with similar ones in the literature (Belarbi *et al.* 2023, Yas and Samadi 2012, Zerrouki *et al.* 2020).

The comparison result considering SS, CC, CF boundary conditions are tabulated in Tables 3-5 respectively. For the simply-simply supported in Tables 3, the results are

Table 4 Non-dimensional critical buckling load $(\bar{N}_{cr})$ of C-C FG-CNTRC beams with different *L/h* values

| L/h | $V^*_{cnt}$ | Reference | Beam | | |
|---|---|---|---|---|---|
| | | | UD | X | O |
| 10 | 0.12 | Present | 0.2877 | 0.3192 | 0.2113 |
| | | Belarbi *et al.* 2023 | 0.2879 | 0.3530 | 0.2113 |
| | 0.17 | Present | 0.4703 | 0.5165 | 0.3470 |
| | | Belarbi *et al.* 2023 | 0.4705 | 0.5648 | 0.3470 |
| | 0.28 | Present | 0.5977 | 0.6189 | 0.4836 |
| | | Belarbi *et al.* 2023 | 0.5981 | 0.7010 | 0.4836 |
| 15 | 0.12 | Present | 0.2179 | 0.2543 | 0.1480 |
| | | Belarbi *et al.* 2023 | 0.2180 | 0.2667 | 0.1480 |
| | | Yas and Samadi 2012 | 0.2139 | 0.2459 | 0.1567 |
| | 0.17 | Present | 0.3485 | 0.4057 | 0.2345 |
| | | Belarbi *et al.* 2023 | 0.3486 | 0.4232 | 0.2345 |
| | | Yas and Samadi 2012 | 0.3442 | 0.4035 | 0.2451 |
| | 0.28 | Present | 0.4622 | 0.5035 | 0.3398 |
| | | Belarbi *et al.* 2023 | 0.4623 | 0.5348 | 0.3398 |
| | | Yas and Samadi 2012 | 0.4556 | 0.5329 | 0.3469 |
| 20 | 0.12 | Present | 0.1655 | 0.2027 | 0.1049 |
| | | Belarbi *et al.* 2023 | 0.1655 | 0.2083 | 0.1049 |
| | 0.17 | Present | 0.2593 | 0.3183 | 0.1620 |
| | | Belarbi *et al.* 2023 | 0.2593 | 0.3261 | 0.1620 |
| | 0.28 | Present | 0.3584 | 0.4125 | 0.2414 |
| | | Belarbi *et al.* 2023 | 0.3585 | 0.4272 | 0.2414 |

Table 5 Non-dimensional critical buckling load $(\bar{N}_{cr})$ of C-F FG-CNTRC beams with different *L/h* values

| L/h | $V^*_{cnt}$ | Reference | Beam | | |
|---|---|---|---|---|---|
| | | | UD | X | O |
| 10 | 0.12 | Present | 0.0633 | 0.0866 | 0.0351 |
| | | Belarbi *et al.* 2023 | 0.0633 | 0.0872 | 0.0351 |
| | 0.17 | Present | 0.0951 | 0.1307 | 0.0521 |
| | | Belarbi *et al.* 2023 | 0.0951 | 0.1315 | 0.0521 |
| | 0.28 | Present | 0.1437 | 0.1903 | 0.0812 |
| | | Belarbi *et al.* 2023 | 0.1437 | 0.1919 | 0.0812 |
| 15 | 0.12 | Present | 0.0312 | 0.0444 | 0.0167 |
| | | Belarbi *et al.* 2023 | 0.0312 | 0.0446 | 0.0167 |
| | | Yas and Samadi 2012 | 0.0312 | 0.0443 | 0.0167 |
| | 0.17 | Present | 0.0463 | 0.0661 | 0.0245 |
| | | Belarbi *et al.* 2023 | 0.0463 | 0.0663 | 0.0245 |
| | | Yas and Samadi 2012 | 0.0463 | 0.0662 | 0.0245 |
| | 0.28 | Present | 0.0721 | 0.1007 | 0.0386 |
| | | Belarbi *et al.* 2023 | 0.0721 | 0.1011 | 0.0385 |
| | | Yas and Samadi 2012 | 0.0721 | 0.1024 | 0.0386 |
| 20 | 0.12 | Present | 0.0183 | 0.0264 | 0.0096 |
| | | Belarbi *et al.* 2023 | 0.0183 | 0.0265 | 0.0096 |
| | 0.17 | Present | 0.0270 | 0.0391 | 0.0140 |
| | | Belarbi *et al.* 2023 | 0.0270 | 0.0391 | 0.0140 |
| | 0.28 | Present | 0.0425 | 0.0607 | 0.0222 |
| | | Belarbi *et al.* 2023 | 0.0425 | 0.0608 | 0.0222 |

Table 6 Dimensionless critical buckling for S-S *X-beam* pattern in exponential distribution

| L/h | $V_{cnt}^{*}$ | Reference | $\bar{N}_{cr}$ | | | | | | | |
|---|---|---|---|---|---|---|---|---|---|---|
| | | | 0.50 | 1 | 1.5 | 2 | 2.3 | 2.5 | 3 | 3.5 |
| 10 | 0.12 | Present | 0.1879 | 0.2026 | 0.2134 | 0.2217 | 0.2258 | 0.2284 | 0.2339 | 0.2387 |
| | | Zerrouki *et al.* (2020) | 0.1860 | 0.1999 | 0.2098 | 0.2174 | 0.2211 | 0.2234 | 0.2283 | 0.2325 |
| | 0.17 | Present | 0.2951 | 0.3183 | 0.3349 | 0.3477 | 0.3541 | - | - | - |
| | | Zerrouki *et al.* (2020) | 0.2928 | 0.3152 | 0.3308 | 0.3426 | 0.3484 | - | - | - |
| 15 | 0.12 | Present | 0.1173 | 0.1298 | 0.1391 | 0.1462 | 0.1498 | 0.1520 | 0.1568 | 0.1608 |
| | | Zerrouki *et al.* (2020) | 0.1166 | 0.1289 | 0.1377 | 0.1445 | 0.1479 | 0.1500 | 0.1544 | 0.1581 |
| | 0.17 | Present | 0.1794 | 0.1989 | 0.2132 | 0.2241 | 0.2296 | - | - | - |
| | | Zerrouki *et al.* (2020) | 0.1788 | 0.1979 | 0.2118 | 0.2223 | 0.2275 | - | - | - |
| 20 | 0.12 | Present | 0.0770 | 0.0866 | 0.0938 | 0.0993 | 0.1022 | 0.1038 | 0.1075 | 0.1106 |
| | | Zerrouki *et al.* (2020) | 0.0768 | 0.0862 | 0.0932 | 0.0986 | 0.1013 | 0.1029 | 0.1064 | 0.1094 |
| | 0.17 | Present | 0.1161 | 0.1307 | 0.1416 | 0.1501 | 0.1543 | - | - | - |
| | | Zerrouki *et al.* (2020) | 0.1158 | 0.1303 | 0.1410 | 0.1493 | 0.1534 | - | - | - |

Table 7 Dimensionless critical buckling load for C-C *beam* pattern in exponential distribution

| L/h | $V_{cnt}^{*}$ | beams | n | | | | | | | |
|---|---|---|---|---|---|---|---|---|---|---|
| | | | 0.5 | 1 | 1.5 | 2 | 2.3 | 2.5 | 3 | 3.5 |
| 10 | 0.12 | O- beam | 0.2432 | 0.2114 | 0.1874 | 0.1684 | 0.1588 | 0.1529 | 0.1400 | 0.1291 |
| | | X- beam | 0.3068 | 0.3192 | 0.3282 | 0.3352 | 0.3385 | 0.3407 | 0.3452 | 0.3494 |
| | 0.17 | O- beam | 0.3992 | 0.3470 | 0.3066 | 0.2743 | 0.2578 | - | - | - |
| | | X- beam | 0.4984 | 0.5166 | 0.5292 | 0.5393 | 0.5443 | - | - | - |
| 15 | 0.28 | O- beam | 0.1771 | 0.1480 | 0.1262 | 0.1094 | 0.1010 | 0.0960 | 0.0852 | 0.0764 |
| | | X- beam | 0.2400 | 0.2542 | 0.2646 | 0.2727 | 0.2768 | 0.2793 | 0.2848 | 0.2894 |
| | 0.12 | O- beam | 0.2825 | 0.2345 | 0.1984 | 0.1704 | 0.1566 | - | - | - |
| | | X- beam | 0.3836 | 0.4057 | 0.4215 | 0.4337 | 0.4399 | - | - | - |
| 20 | 0.17 | O- beam | 0.1297 | 0.1049 | 0.0870 | 0.0735 | 0.0670 | 0.0632 | 0.0551 | 0.0486 |
| | | X- beam | 0.1880 | 0.2027 | 0.2134 | 0.2217 | 0.2258 | 0.2284 | 0.2339 | 0.2387 |
| | 0.28 | O- beam | 0.2019 | 0.1620 | 0.1331 | 0.1116 | 0.1011 | - | - | - |
| | | X- beam | 0.2951 | 0.3183 | 0.3349 | 0.3477 | 0.3540 | - | - | - |

compared with (Belarbi *et al*. 2023) in the case of (L/h=10 and 20) and the comparison extends to the two works in the case of (L/h=15) with (Yas and Samadi 2012, Zerrouki *et al*. 2020). As observed, there is very clear that the present results show a good agreement with those obtained by them.

Moreover, another comparison is made for the clamped-clamped supported in Tables 4 and clamped-free supported in Tables 5 when the results are compared with (Belarbi *et al*. 2023 and Yas and Samadi 2012). As noticed, that this comparison is also good for the different distribution of carbon nanotubes.

It should be mentioned that The UD-CNTRC and FG-CNTRC beams had the same mass fraction of carbon nanotubes, which was maintained by adjusting the volume fraction of CNTs in each beam. Additionally, the critical buckling load changes due to the distribution of carbone nanotubes. The (X-CNT) reinforced beams are the clear higher in terms of dimensionless critical buckling loads, compared with other reinforcement types (UD-CNT, O-CNT). It should be concluded that the highest critical buckling loads remarked in X-CNT beams are attributed to the high concentration of carbon nanotubes at the bottom and top faces of the beam, which results in enhanced of reinforcement and stiffness.

The elevated frequencies are observed in C-C beams, compared by C-H and C-F beams, respectively, at every volume fraction. Thos highest values are attributed to boundary conditions that provide greater support and stiffness to the beams.

Also comparing the results of the dimensionless critical buckling load of the S-S beam with the results of (Zerrouki *et al*. 2020) in Table 6, the results are presented for the S-S X-beam pattern in such a way that a comparison with reference is possible. It can be seen that is an excellent agreement between the obtained results in this paper and those reported in (Zerrouki *et al*. 2020). It is clear that the

Table 8 Dimensionless critical buckling load for C-F *beam* pattern in exponential distribution

| L/h | $V^*_{cnt}$ | beams | n | | | | | | | |
|---|---|---|---|---|---|---|---|---|---|---|
| | | | 0.5 | 1 | 1.5 | 2 | 2.3 | 2.5 | 3 | 3.5 |
| 10 | 0.12 | O- beam | 0.0460 | 0.0351 | 0.0278 | 0.0227 | 0.0203 | 0.0189 | 0.0161 | 0.0139 |
| | | X- beam | 0.0770 | 0.0866 | 0.0938 | 0.0994 | 0.1021 | 0.1038 | 0.1075 | 0.1106 |
| | 0.17 | O- beam | 0.0687 | 0.0521 | 0.0410 | 0.0331 | 0.0295 | - | - | - |
| | | X- beam | 0.1161 | 0.1307 | 0.1416 | 0.1501 | 0.1543 | - | - | - |
| 15 | 0.28 | O- beam | 0.0222 | 0.0167 | 0.0131 | 0.0105 | 0.0094 | 0.0087 | 0.0074 | 0.0064 |
| | | X- beam | 0.0389 | 0.0444 | 0.0486 | 0.0519 | 0.0536 | 0.0546 | 0.0568 | 0.0586 |
| | 0.12 | O- beam | 0.0328 | 0.0245 | 0.0190 | 0.0153 | 0.0135 | - | - | - |
| | | X- beam | 0.0578 | 0.0661 | 0.0724 | 0.0773 | 0.0797 | - | - | - |
| 20 | 0.17 | O- beam | 0.0129 | 0.0096 | 0.0075 | 0.0060 | 0.0054 | 0.0050 | 0.0042 | 0.0036 |
| | | X- beam | 0.0230 | 0.0264 | 0.0291 | 0.0311 | 0.0322 | 0.0328 | 0.0342 | 0.0353 |
| | 0.28 | O- beam | 0.0189 | 0.0140 | 0.0109 | 0.0087 | 0.0077 | - | - | - |
| | | X- beam | 0.0340 | 0.0391 | 0.0430 | 0.0460 | 0.0476 | - | - | - |

of CNT volume fractions reaches to $2V^*_{cnt}$. In this work the

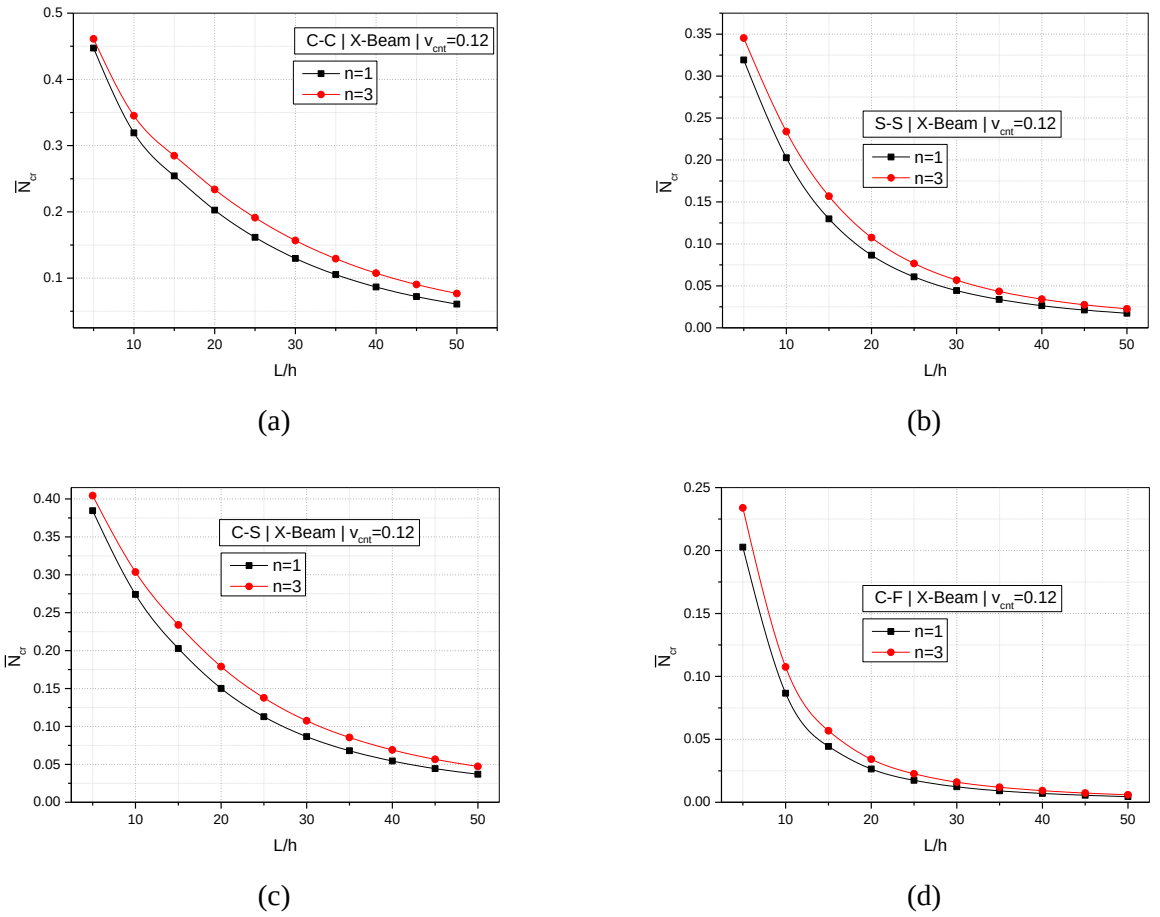


Fig. 4 Effect of degree of exponent (n) and the aspect ratio of X-beam on the dimensionless critical buckling with various boundary conditions ($V^*_{cnt}$=0.12)

increasing of exponent degree (n) result the increase of critical buckling load for both volume fraction. It can be seen that the increase of the length of the beam decrease the critical buckling loads.

In the linear distribution of FG-CNTRC the maximum maximum of CNT volume fractions in the nonlinear distribution reach to$(n + 1)V^*_{cnt}$. For this reason, we have chosen the degree of exponent (n) in which the CNT volume fraction does not exceed the value 0.56 which is the

maximum value in the linear distribution.

Table 7 and 8 shows the dimensionless critical buckling load of FG-CNT beam with various boundary conditions, various aspect ratios L/h and various volume fractions. In this case, aspect ratio L/h is set to 10, 15 and 20. The booth configuration O-beam and X-beam have been considered. The results are obtained for different volume fractions with exponential distribution. It is found that the value of the dimensionless critical buckling loads obtained in parabolic distribution decreasing rapidly with the increase of the aspect ratio L/h (the ratio of material length scale parameter to thickness). Also, by increasing the volume fractions, a dimensionless critical buckling load of FG-CNT beam will be increase for both configuration O-beam and X-beam. A significant increase is observed for the X-beam configuration. But for a comparison between the different configurations for the same volume fraction, we note that the concentration of the carbon nanotubes on the upper and lower faces increases the dimensionless critical load and the concentration of these nanotubes at the core of the beam reduces the dimensionless critical load. That is to say, the increase in the coefficient "n" in the X-beam configuration makes the beam more rigid; on the other hand, this concentration makes the O-beam beam more flexible.

Also, it is demonstrated that the critical buckling load is maximum for clamped-clamped (CC) boundary conditions in comparison with other types. The embedding conditions at both ends completely prevent the rotation of the beams and increase the moment of inertia of the beam. This means that the beam is forced to bend in an arc shape, which distributes the load over a greater length and increases the buckling resistance. In other words, the (CC) boundary induces more bending rigidity in the beam.

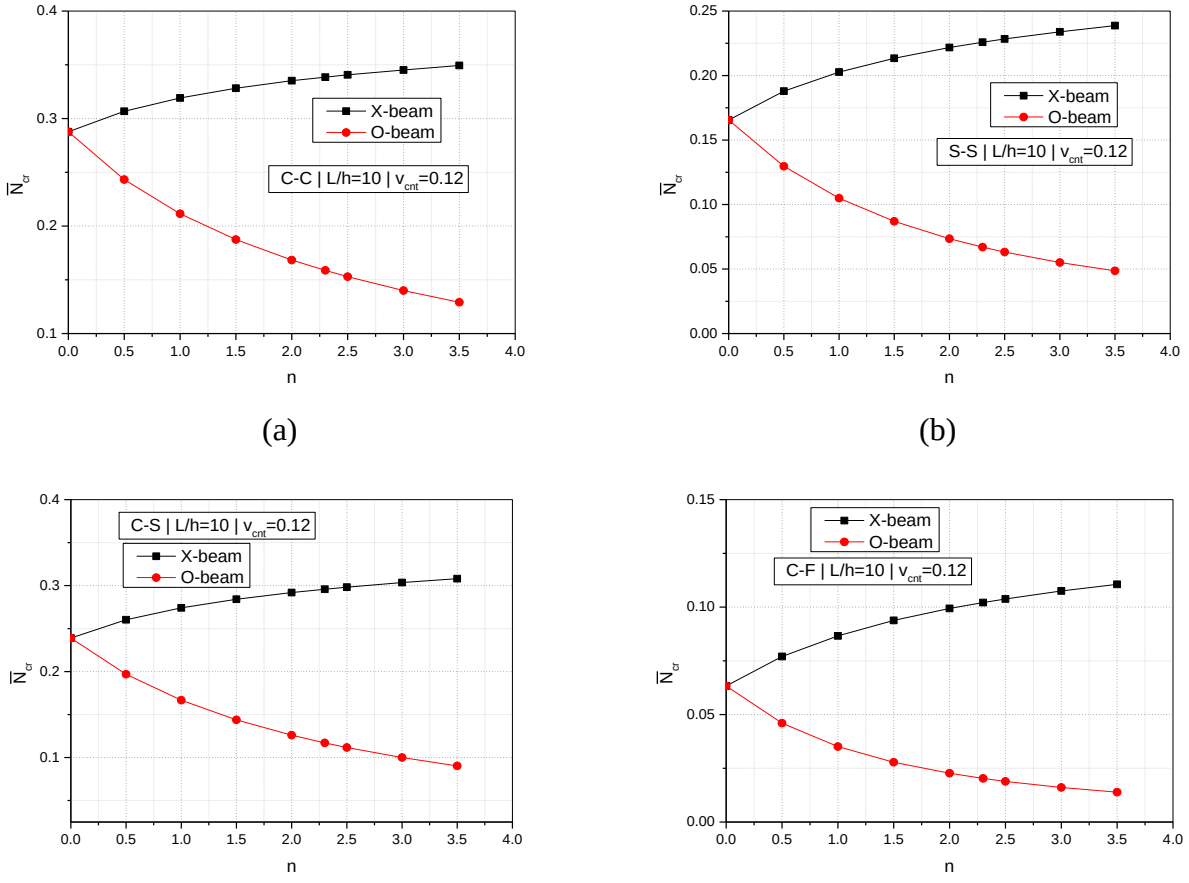


Fig. 5 Effect of degree of exponent n and the type of distribution on the critical buckling loads

Fig. 4 (a-d) examines the effect of exponent degree (*n*) and the aspect ratio of *X-beam* on the dimensionless critical buckling load and illustrates the effect of different boundary conditions. The results in those figures are obtained by using the volume fraction ($V^*_{cnt}$=0.12). As can be seen, the dimensionless critical buckling load of the X-beam with CC boundary condition is about twice that with CF boundary condition. In addition, the dimensionless critical buckling load for the beam with CC boundary condition is about 18% to 40% higher than that of SS and CS conditions respectively. It is for this reason that the clamped-clamped boundary condition improves the rigidity of the structure and hence the critical buckling load increases.

For any boundary condition, It is clear that the value of the dimensionless critical buckling loads obtained in parabolic (n=3) distribution is higher than that obtained in a linear distribution (n=1). This explains the concentration

effect of the carbon nanotubes on the upper and lower faces of beam. Moreover, from these figures it can be seen that as the aspect ratio increase, the dimensionless critical buckling decrease.

Figs. 5 (a-d) illustrate the variation of the critical buckling of FG-CNTRC beams with X-beam and O-beam distribution of CNT with different boundary conditions. The results in this figure are obtained by using the constant value of CNT volume fraction $V_{cnt}^{*}$ = *0.12* and aspect ratio *L/h=10*. The degree of exponent (*n*) is varied for values (0 - 3.5). From these figures, it can be seen that as the degree of exponent parameter increases, the critical buckling load decrease for the case with O-beam and increase for the case with X-beam. This inconsistency in results is due to the concentration of carbon nanotube in the polymer matrix. In the case of distribution X-beam, the concentration of carbon nanotube is very high on the upper and lower faces of beam which makes the beam more rigid. But in the case of distribution O-beam, the concentration of carbon nanotube is very high in the core of the beam which makes the beam more flexible. This comparison shows that the best distribution with respect to buckling is the case of X-beam. As we concluded previously, the clamped-clamped boundary condition improves the rigidity of the structure and hence the critical buckling load increases.

To investigate the effect of CNT volume fraction, tow values are considered 0.12 and 0.17 in figure 6 for four boundary conditions. As can be seen, when CNT volume fraction enlarge the dimensionless critical buckling loads increase

For an increase in the volume fraction of 0.05 we observe a variation in the dimensionless critical load of 53% for a concentration of n=0.5. This increase becomes less significant when n increases. We conclude that the increase in the volume fraction and the concentration coefficient n leads to stiffening the beam. This analysis applies to various boundary conditions. Also, it can be seen that the critical buckling load for clamped-clamped (CC) boundary conditions is higher than that of other boundary conditions.

## 7. Conclusions

The present numerical research has studied the buckling of functionally graded polymer beam which is composed of (10, 10) carbon nanotube and polymeric matrix (PMMA). The main benefit of the proposed exponential power law distribution is the impact of nonlinear distribution on both mechanical and economic aspects. After performing comparison studies with data reported by other authors. The main conclusions can be stated as following:

• It is observed that the influences of exponential distribution in the beam play an important role to improve the rigidity of beam compared to the linear distribution.

• It can be seen that the critical buckling load for clamped-clamped (CC) boundary conditions was greater than for other boundary conditions.

• Compared with other reinforcement types (UD-CNT, O-CNT), the (X-CNT) reinforced beams are the highest critical buckling loads, It should be concluded that the high concentration of carbon nanotubes at the bottom and top faces of the beam increase the rigidity.

• The dimensionless critical buckling loads obtained in parabolic distribution decreasing rapidly with the increase of the ratio of material length scale parameter to thickness.

## Acknowledgment

The authors would like to acknowledge the support provided by the Directorate General for Scientific Research and Technological Development (DGRSDT).

## References

Alhaifi, K., Khorshidvand, A.R., Al-Masoudy, M.M., Arshid, E. and Madani, S.H. (2023), "A shooting method for buckling and post-buckling analyses of FGSP circular plates considering various patterns of Pores' placement", *Struct. Eng. Mech.*, **85**(3), 419-432. https://doi.org/10.12989/sem.2023.85.3.419

Arani, A.J. and Kolahchi, R. (2016), "Buckling analysis of embedded concrete columns armed with Carbonnanotubes", *Comput. Concr.*, **17**(5), 567-578. https://doi.org/10.12989/cac.2016.17.5.567

Belarbi, M.O., Salami, S.J., Garg, A., Daikh, A.A., Houari, M.S. A., Dimitri, R. and Tornabene, F. (2023), "Mechanical behavior analysis of FG-CNT-reinforced polymer composite beams via a hyperbolic shear deformation theory", *Continuum Mech. Thermodyn.*, **35**, 497-520. https://doi.org/10.1007/s00161-023-01191-2

Chang, G., Huang, H. and Li, Z. (2024). "Systematic failure mechanism of an FGMs polyhedral arched liner under a fire disaster environment", *Eng. Struct.*, **305**, 117655. https://doi.org/10.1016/j.engstruct.2024.117655

Chang, G. and Li, Z. (2024). "Systematic schemes for buckling analyses of a subsea bio-inspired non-circular FGM polyhedral liner with an arch invert", *Ocean Eng.*, **300**, 117484. https://doi.org/10.1016/j.oceaneng.2024.117484

Ebrahimi, F. and Habibi, S. (2017). "Low-velocity impact response of laminated FG-CNT reinforced composite plates in thermal environment", *Adv. Nano Res.*, **5**(2), 69. https://doi.org/10.12989/anr.2017.5.2.069

Dresselhaus, M.S. and Avouris, P. (2001), *Introduction to Carbon Materials Research*, In *Carbon Nanotubes, Topics Appl. Phys.*, **80**, 1-9, Springer, Berlin, Heidelberg.

Eltaher, M.A., Almalki, T.A., Ahmed, K.I. and Almitani, K.H. (2019), "Characterization and behaviors of single walled carbon nanotube by equivalent-continuum mechanics approach", *Adv. Nano Res.*, **7**(1), 39-49, http://doi.org/10.12989/anr.2019.7.1.039

Jamali, M., Shojaee, T., Mohammadi, B. and Kolahchi, R. (2019), "Cut out effect on nonlinear post-buckling behavior of FG-CNTRC micro plate subjected to magnetic field via FSDT", *Adv. Nano Res*, **7**(6), 405-417. https://doi.org/10.12989/anr.2019.7.6.405

Han, Y. and Elliott, J. (2007), "Molecular dynamics simulations of the elastic properties of polymer/carbon nanotube composites", *Comput. Mater. Sci.*, **39**(2), 315-323. https://doi.org/10.1016/j.commatsci.2006.06.011

Iijima, S. (1991), "Helical microtubules of graphitic carbon", *Nature*, **354**(6348), 56-58. https://doi.org/10.1038/354056a0

Jiang B., Liu C., Zhang C., Liang R. and Wang B. (2009), "Maximum nanotube volume fraction and its effect on overall elastic properties of nanotube-reinforced composites", *Compos.*

*Part B*, **40**, 212-217. https://doi.org/10.1016/j.compositesb.2008.11.003

Jin, Y. and Yuan, F.G. (2003), "Simulation of elastic properties of single-walled carbon nanotubes", *Compos. Sci. Technol.*, **63**(11), 1507-1515. https://doi.org/10.1016/S0266-3538(03)00074-5

Kiani, Y. (2017), "Buckling of FG-CNT-reinforced composite plates subjected to parabolic loading", *Acta Mechanica*, **228**(4), 1303-1319, https://doi.org/10.1007/s00707-016-1781-4.

Kiani, Y., Bagherizadeh, E. and Eslami, M.R. (2011), "Thermal buckling of clamped thin rectangular FGM plates resting on Pasternak elastic foundation (Three approximate analytical solutions)", *Zeitschr. Angwe. Math. Mech*, **91**(7), 581-593. https://doi.org/10.1002/zamm.201000184.

Kolahchi, R., Keshtegar, B. and Fakhar, M.H. (2020). "Optimization of dynamic buckling for sandwich nanocomposite plates with sensor and actuator layer based on sinusoidal-visco-piezo-elasticity theories using Grey Wolf algorithm", *J. Sandw. Struct. Mater.*, **22**(1), 3-27. https://doi.org/10.1177/1099636217731071

Li, Z., Zhang, Q., Shen, H., Xiao, X., Kuai, H. and Zheng, J. (2023). "Buckling performance of the encased functionally graded porous composite liner with polyhedral shapes reinforced by graphene platelets under external pressure", *Thin Wall. Struct.*, **183**, 110370. https://doi.org/10.1016/j.tws.2022.110370

Mallek, H., Jrad, H., Wali, M., Kessentini, A., Gamaoun, F. and Dammak, F. (2020), "Dynamic analysis of functionally graded carbon nanotube-reinforced shell structures with piezoelectric layers under dynamic loads", *J. Vib. Control*, **26**(13-14), 1157-1172. https://doi.org/10.1177/1077546319892753.

Heidari, F., Afsari, A. and Janghorban, M. (2020), "Several models for bending and buckling behaviors of FG-CNTRCs with piezoelectric layers including size effects", *Adv. Nano Res.*, **9**(3), 193-210. https://doi.org/10.12989/anr.2020.9.3.193

Mayandi, K. and Jeyaraj, P. (2015), "Bending, buckling and free vibration characteristics of FG-CNT polymer composite beam under non-uniform thermal load", *J. Mater. Des. Appl.*, **229**, 13-28. https://doi.org/10.1177/1464420713493720

Mehar, K. and Panda, S.K. (2018), "Thermal free vibration behavior of FG-CNT reinforced sandwich curved panel using finite element method", *Polym. Compos.*, **39**, 2751-2764. https://doi.org/10.1002/pc.24266

Mellouli, H., Jrad, H., Wali, M. and Dammak, F. (2020), "Free vibration analysis of FG-CNTRC shell structures using the meshfree radial point interpolation method", *Comput. Math. Appl.*, **79**(11), 3160-3187,. https://doi.org/10.1016/j.camwa.2020.01.015.

Mirzaei, M. and Kiani, Y. (2016), "Thermal buckling of temperature dependent FG-CNT reinforced composite plates", *Meccanica*, **51**, 2185-2201. https://doi.org/10.1007/s11012-015-0348-0

Mohammadimehr, M., Shahedi, S. and Rousta Navi, B. (2017), "Nonlinear vibration analysis of FG-CNTRC sandwich Timoshenko beam based on modified couple stress theory subjected to longitudinal magnetic field using generalized differential quadrature method", *Proceedings of the Institution of Mechanical Engineers, Part C: J. Mech. Eng. Sci.*, **231**(20), 3866-3885. https://doi.org/10.1177/0954406216653622

Peddieson, J., Buchanan, G.R. and McNitt, R.P. (2003), "Application of nonlocal continuum models to nanotechnology" *Int. J. Eng. Sci.*, **41**(3-5), 305-312. https://doi.org/10.1016/S0020-7225(02)00210-0

Phung-Van, P., Thanh, C.L., Nguyen-Xuan, H. and Abdel-Wahab, M. (2018), "Nonlinear transient isogeometric analysis of FG-CNTRC nanoplates in thermal environments", *Compos. Struct.*, **201**, 882-892. https://doi.org/10.1016/j.compstruct.2018.06.087.

Ru, C.Q. (2000), "Elastic buckling of single-walled carbon nanotube ropes under high pressure", *Phys. Rev. B*, **62**(15), 10405. https://doi.org/10.1103/PhysRevB.62.10405.

She, G.L., Yuan, F.G., Ren, Y.R. and Xiao, W.S. (2017), "On buckling and postbuckling behavior of nanotubes", *Int. J. Eng. Sci.*, **121**, 130-142. https://doi.org/10.1016/j.ijengsci.2017.09.005

Shen, H.S. (2009), "Nonlinear bending of functionally graded carbon nanotube-reinforced composite plates in thermal environments", *Compos. Struct.*, **91**(1), 9-19. https://doi.org/10.1016/j.compstruct.2009.04.026.

Simsek M. (2010), "Fundamental frequency analysis of functionally graded beams by using different higher-order beam theories", *Nuclear Eng. Des.*, **240**, 697-705. http://doi.org/10.1016/j.nucengdes.2009.12.013

Tagrara, S.H., Benachour, A., Bouiadjra, M.B. and Tounsi, A. (2015), "On bending, buckling and vibration responses of functionally graded carbon nanotube-reinforced composite beams", *Steel Compos. Struct.*, **19**(5), 1259-1277. https://doi.org/10.12989/scs.2015.19.5.1259.

Tlidji, Y., Benferhat, R., Daouadji, T. H., Tounsi, A. and Trinh, L. C. (2022). "Free vibration analysis of FGP nanobeams with classical and non-classical boundary conditions using State-space approach", *Adv. Nano Res.*, **13**(5), 453. https://doi.org/10.12989/anr.2022.13.5.453

Vodenitcharova, T. and Zhang, L.C. (2006), "Bending and local buckling of a nanocomposite beam reinforced by a single-walled carbon nanotube", *J. Sol. Struct.*, **43**(10), 3006-3024. https://doi.org/10.1016/j.ijsolstr.2005.05.014

Wang, Q., Varadan, V. K. and Quek, S. T. (2006), "Small scale effect on elastic buckling of carbon nanotubes with nonlocal continuum models", *Phys. Lett. A*, **357**(2), 130-135. https://doi.org/10.1016/j.physleta.2006.04.026.

Weon, J.I. (2009), "Mechanical and thermal behavior of polyamide-6/clay nanocomposite using continuumbased micro-mechanical modeling", *Macromol. Res.*, **17**(10), 797-806. https://doi.org/10.1007/BF03218617.

Wu, H., Kitipornchai, S. and Yang, J. (2015), "Free vibration and buckling analysis of sandwich beams with functionally graded carbon nanotube-reinforced composite face sheets", *J. Struct. Stab. Dyn.*, **15**(7), 1540011. https://doi.org/10.1142/S0219455415400118

Yang, J., Ke, L.L. and Feng, C. (2015), "Dynamic buckling of thermo-electro-mechanically loaded FGCNTRC beams", *J. Struct. Stab. Dyn.*, **15**(8), 1540017. https://doi.org/10.1142/S0219455415400179

Yas, M. H. and Samadi, N. (2012), "Free vibrations and buckling analysis of carbon nanotube-reinforced composite Timoshenko beams on elastic foundation", *Int. J. Press. Vessels Pip.*, **98**, 119-128. https://doi.org/10.1016/j.ijpvp.2012.07.012.

Zenkour, A.M. (2018), "Modified couple stress theory for micro-machined beam resonators with linearly varying thickness and various boundary conditions", *Arch. Mech. Eng.*, **65**(1), 43-64. https://doi.org/10.24425/119409.

Zerrouki, R., Karas, A. and Zidour, M. (2020), "Critical buckling analyses of nonlinear FG-CNT reinforced nano-composite beam", *Adv. Nano Res.*, **9**(3), 211-220. https://doi.org/10.12989/anr.2020.9.3.211

Zghal, S., Ataoui, D. and Dammak, F (2020), "Static bending analysis of beams made of functionally graded porous materials", *Mech. Based Des. Struct.*, **50**(3),1-18. https://doi.org/10.1080/15397734.2020.1748053.

Zhang, L.W., Lei, Z.X. and Liew, K.M. (2015), "Buckling analysis of FG-CNT reinforced composite thick skew plates using an element-free approach", *Compos. Part B Eng.*, **75**, 36-46. https://doi.org/10.1016/j.compositesb.2015.01.033.

Zhang, L.W., Liew, K.M. and Reddy, J.N. (2016), "Postbuckling of carbon nanotube reinforced functionally graded plates with

edges elastically restrained against translation and rotation under axial compression", *Comput. Meth. Appl. Mech. Eng.*, **298**, 1-28. https://doi.org/10.1016/j.cma.2015.09.016.

Zhang, S., Bu, R., Zhang, Z., Gao, L. and Li, Z. (2024). "A systematic model for the mechanical behavior of thin-walled composite FGM pipelines subjected to strike-slip faults in geohazard area", *Thin Wall. Struct.*, 112135. https://doi.org/10.1016/j.tws.2024.112135

Zhu, P., Lei, Z.X. and Liew, K.M. (2012), "Static and free vibration analyses of carbon nanotube reinforced composite plates using finite element method with first order shear deformation plate theory", *Compos. Struct.*, **94**, 1450-1460. https://doi.org/10.1016/j.compstruct.2011.11.010

Xiao, X., Bu, G., Ou, Z. and Li, Z. (2022), "Nonlinear in-plane instability of the confined FGP arches with nanocomposites reinforcement under radially-directed uniform pressure", *Eng. Struct.*, **252**, 113670. https://doi.org/10.1016/j.engstruct.2021.113670

Xiao, X., Zhang, Q., Chang, G., Liu, Y. and Li, Z. (2024), "Structural optimization model of confined polyhedral composite subsea pipelines under pressure and thermal fields", *Marine Struct.*, **94**, 103548. https://doi.org/10.1016/j.marstruc.2023.103548

Xiao, X., Zhang, Q., Zheng, J. and Li, Z. (2023), "Analytical model for the nonlinear buckling responses of the confined polyhedral FGP-GPLs lining subjected to crown point loading", *Eng. Struct.*, **282**, 115780. https://doi.org/10.1016/j.engstruct.2023.115780

*CC*